

ENHANCED STRAIN METHODS FOR ELASTICITY PROBLEMS

F. Auricchio^{a,c}, L. Beirão da Veiga^b, C. Lovadina^{b,c} and A. Reali^{a,d}

^aDipartimento di Meccanica Strutturale
Università di Pavia, I-27100 Pavia, Italy
e-mails: auricchio@unipv.it, alessandro.reali@unipv.it
web page: <http://www.unipv.it/dms/auricchio>

^bDipartimento di Matematica
Università di Pavia, I-27100 Pavia, Italy
e-mails: beirao@dimat.unipv.it, lovadina@dimat.unipv.it
web page: <http://www-dimat.unipv.it/lovadina>

^cIstituto di Matematica Applicata e Tecnologie Informatiche del CNR
I-27100 Pavia, Italy

^dEuropean School for Advanced Studies in Reduction of Seismic Risk (ROSE School)
Università di Pavia, I-27100 Pavia, Italy

Key words: Finite Element Methods, Enhanced Strain Technique, Finite Strain Elasticity Problems, Stability Analysis.

Abstract. *The so-called Enhanced Strain Technique for the approximation of homogeneous neo-Hookean elasticity problems is considered within the framework of the displacement/pressure variational formulation. Two triangular low-order schemes for nearly-incompressible small strain problems are presented, together with some numerical result. Moreover, a simple model problem for the large strain regime is proposed. The model problem is used to investigate the numerical stability of the mixed-enhanced quadrilateral Q4E6/Q4 element introduced in [15] and [16].*

1 INTRODUCTION

The aim of this paper is to report some recent results concerning the *Enhanced Strain Technique* for elasticity problems, and developed in full details in [1, 2].

Introduced by Simo and Rifai (cf. [22]), the Enhanced Strain Technique consists in augmenting the space of discrete strains with local functions, which may not derive from admissible displacements. A suitable choice of these additional modes can improve the numerical performance of low-order elements and, more importantly, it can greatly alleviate the well-known *volumetric locking* phenomenon in the nearly-incompressible regime.

We here focus on enhanced strain finite elements based on the so-called displacement/pressure formulation for elasticity problems (cf. e.g. [15, 16]), considering, for simplicity, a homogeneous neo-Hookean material. Within this framework, we will consider the following two cases.

- *The small deformation case* (Section 3). We present two triangular elements, for which a complete stability and convergence analysis has been developed in [1]. Both the schemes are based on piecewise linear and continuous approximations for the displacement and the pressure unknowns. We also report some numerical results which confirm the theoretical predictions.
- *The finite strain incompressible elasticity case* (Section 4). Following [2], we present a simple finite strain elastic bidimensional problem for which not only it is possible to compute the solution in closed form but it is also possible to draw some indications on the solution stability. We then consider the discretized problem by means of the $Q4E6/Q4$ mixed-enhanced finite element (see [16]), which has been proved to be stable and well performing in linear elasticity (cf. [11]). Afterwards, we report some theoretical considerations on the stability limits of the discrete problem, showing that the $Q4E6/Q4$ element fails to reproduce the continuum stability features. We remark that this phenomenon has been already observed in [16]. Furthermore, we perform some numerical simulations to investigate the whole stability range of the scheme at hand.

Finally, we remark that several contributions on the applications of the Enhanced Strain Technique are nowadays available in the literature, ranging from Engineering-oriented studies (see [3, 14, 19, 20, 21, 24], for instance) to more theoretical investigations (see [5, 12, 18], for instance).

2 THE FINITE STRAIN ELASTICITY PROBLEM

In this work we adopt the so-called *material description* to study the finite strain elasticity problem for a homogeneous neo-Hookean material (cf. [6, 8, 10, 13], for example). Accordingly, we suppose that we are given a *reference configuration* $\Omega \subset \mathcal{R}^d$ for a d -dimensional bounded material body \mathcal{B} . In the framework of the Hellinger-Reissner variational principle, the elastic problem may be written as follows:

$$\left\{ \begin{array}{l} \text{Find } (\hat{\mathbf{u}}, \hat{p}) \in \hat{U} \times \hat{P} \text{ such that} \\ \mu \int_{\Omega} \hat{\mathbf{F}} : \nabla \mathbf{v} + \int_{\Omega} (\hat{p} - \mu) \hat{\mathbf{F}}^{-T} : \nabla \mathbf{v} - \int_{\Omega} \mathbf{b} \cdot \mathbf{v} = \mathbf{0} \quad \forall \mathbf{v} \in U \\ \int_{\Omega} \left(\ln \hat{J} - \frac{\hat{p}}{\lambda} \right) q = 0 \quad \forall q \in P . \end{array} \right. \quad (1)$$

Above, $\hat{\mathbf{u}}$ and \hat{p} represent the displacement and pressure-like unknown fields, respectively. Moreover, $\hat{\mathbf{F}} = \mathbf{I} + \nabla \hat{\mathbf{u}}$ is the deformation gradient whose determinant is $\hat{J} = \det \hat{\mathbf{F}}$, λ and μ are positive material constants, and \mathbf{b} represents the given load. Finally, \hat{U} and \hat{P} are the admissible displacement and pressure spaces, while U and P are the corresponding variation spaces. In residual form problem (1) can be written as

$$\left\{ \begin{array}{l} \text{Find } (\hat{\mathbf{u}}, \hat{p}) \in \hat{U} \times \hat{P} \text{ such that} \\ \mathcal{R}_u((\hat{\mathbf{u}}, \hat{p}), \mathbf{v}) = \mathbf{0} \quad \forall \mathbf{v} \in U \\ \mathcal{R}_p((\hat{\mathbf{u}}, \hat{p}), q) = 0 \quad \forall q \in P , \end{array} \right. \quad (2)$$

where

$$\left\{ \begin{array}{l} \mathcal{R}_u((\hat{\mathbf{u}}, \hat{p}), \mathbf{v}) := \mu \int_{\Omega} \hat{\mathbf{F}} : \nabla \mathbf{v} + \int_{\Omega} (\hat{p} - \mu) \hat{\mathbf{F}}^{-T} : \nabla \mathbf{v} - \int_{\Omega} \mathbf{b} \cdot \mathbf{v} \\ \mathcal{R}_p((\hat{\mathbf{u}}, \hat{p}), q) := \int_{\Omega} \left(\ln \hat{J} - \frac{\hat{p}}{\lambda} \right) q . \end{array} \right. \quad (3)$$

We now derive the linearization of problem (1) around a generic point $(\hat{\mathbf{u}}, \hat{p})$. Observing that

$$D\hat{\mathbf{F}}^{-T}(\hat{\mathbf{u}})[\mathbf{u}] = -\hat{\mathbf{F}}^{-T}(\nabla \mathbf{u})^T \hat{\mathbf{F}}^{-T} \quad \forall \mathbf{u} \in U , \quad (4)$$

we easily get the problem for the *infinitesimal* increment (\mathbf{u}, p)

$$\left\{ \begin{array}{l} \text{Find } (\mathbf{u}, p) \in U \times P \text{ such that} \\ \mu \int_{\Omega} \nabla \mathbf{u} : \nabla \mathbf{v} + \int_{\Omega} (\mu - \hat{p}) (\hat{\mathbf{F}}^{-1} \nabla \mathbf{u})^T : \hat{\mathbf{F}}^{-1} \nabla \mathbf{v} \\ + \int_{\Omega} p \hat{\mathbf{F}}^{-T} : \nabla \mathbf{v} = -\mathcal{R}_u((\hat{\mathbf{u}}, \hat{p}), \mathbf{v}) \quad \forall \mathbf{v} \in U \\ \int_{\Omega} \left(\hat{\mathbf{F}}^{-T} : \nabla \mathbf{u} - \frac{1}{\lambda} p \right) q = -\mathcal{R}_p((\hat{\mathbf{u}}, \hat{p}), q) \quad \forall q \in P . \end{array} \right. \quad (5)$$

Remark 2.1 *Since problem (5) is the linearization of problem (1) (or equivalently (2)), it can be interpreted as the generic step of a Newton-like iteration procedure for the solution of the non-linear problem (1).*

3 THE SMALL DEFORMATION CASE AND SOME TRIANGULAR ENHANCED STRAIN ELEMENTS

Taking $(\hat{\mathbf{u}}, \hat{p}) = (0, 0)$ in (5), we immediately recover the classical linear elasticity problem for small deformations, i.e.

$$\left\{ \begin{array}{l} \text{Find } (\mathbf{u}, p) \in U \times P \text{ such that} \\ 2\mu \int_{\Omega} \boldsymbol{\varepsilon}(\mathbf{u}) : \boldsymbol{\varepsilon}(\mathbf{v}) + \int_{\Omega} p \operatorname{div} \mathbf{v} = \int_{\Omega} \mathbf{b} \cdot \mathbf{v} \quad \forall \mathbf{v} \in U \\ \int_{\Omega} \left(\operatorname{div} \mathbf{u} - \frac{1}{\lambda} p \right) q = 0 \quad \forall q \in P, \end{array} \right. \quad (6)$$

where $\boldsymbol{\varepsilon}(\cdot)$ denotes the symmetric gradient operator. For simplicity, we here consider the case of homogeneous Dirichlet boundary conditions on the whole $\partial\Omega$, so that $U = H_0^1(\Omega)^2$ and $P = L^2(\Omega)/\mathbf{R}$. It is now well-established (cf. [4, 7, 9]) that the finite element analysis of problem (6) requires some care in the case of nearly-incompressible materials ($\lambda \gg \mu$), in order to overcome the so-called *volume locking phenomenon*. Several methods have been proposed, analyzed and proved to be efficient in actual computations (cf. [4, 7, 9] and the references therein). Among them, there are the ones based on the *Enhanced Strain Technique*, whose basic idea is briefly recalled below.

As usual, given a regular (triangular or quadrilateral) mesh \mathcal{T}_h of Ω , h being the mesh-size, we choose a finite element space $U_h \subset U$ for the approximation of the displacements, and a finite element space $P_h \subset P$ for the pressure field.

An *Enhanced Strain Method* in this context can be seen as a scheme for which the strains arising from the displacements are “enriched” by means of some additional modes. Therefore, we introduce a further finite element space E_h of symmetric tensors, and we solve the problem:

Find $(\mathbf{u}_h, \tilde{\boldsymbol{\varepsilon}}_h, p_h) \in U_h \times E_h \times P_h$ such that

$$\left\{ \begin{array}{l} 2\mu \int_{\Omega} (\boldsymbol{\varepsilon}(\mathbf{u}_h) + \tilde{\boldsymbol{\varepsilon}}_h) : (\boldsymbol{\varepsilon}(\mathbf{v}_h) + \tilde{\boldsymbol{\tau}}_h) + \int_{\Omega} p_h (\operatorname{div} \mathbf{v}_h + \operatorname{tr} \tilde{\boldsymbol{\tau}}_h) = \int_{\Omega} \mathbf{b} \cdot \mathbf{v}_h \\ \int_{\Omega} q_h (\operatorname{div} \mathbf{u}_h + \operatorname{tr} \tilde{\boldsymbol{\varepsilon}}_h) - \lambda^{-1} \int_{\Omega} p_h q_h = 0, \end{array} \right. \quad (7)$$

for every $(\mathbf{v}_h, \tilde{\boldsymbol{\tau}}_h) \in U_h \times E_h$ and for every $q_h \in P_h$. Above and in the sequel, we denote with “tr” the trace operator acting on tensors.

3.1 Examples of triangular elements

We now introduce two sets of enhanced strains to be used in connection with *triangular* elements, already presented and briefly analyzed in [12]. We thus suppose to have a

regular triangular mesh \mathcal{T}_h of Ω . The schemes we are going to present are both based on the following choice of spaces:

$$U_h = \{v_h \in V : v_{h|T} \in \mathcal{P}_1(T) \quad \forall T \in \mathcal{T}_h\} , \quad (8)$$

$$P_h = \{q_h \in H^1(\Omega) : q_{h|T} \in \mathcal{P}_1(T) \quad \forall T \in \mathcal{T}_h\} , \quad (9)$$

where $\mathcal{P}_1(T)$ is the space of linear functions defined on T .

Before introducing the two sets of enhanced strains, which will give rise to two finite element schemes (named in the sequel as $T3E4(I)/T3$ and $T3E4(II)/T3$ element, respectively), we define a global Cartesian system of coordinates (x, y) in Ω . Furthermore, for each triangle $T \in \mathcal{T}_h$, let (x_T, y_T) be the coordinates of its barycenter, and define on T a *local* Cartesian system of coordinates by simply setting

$$\bar{x} = x - x_T , \quad \bar{y} = y - y_T . \quad (10)$$

We are now ready to present our strain enhancements.

- $T3E4(I)/T3$ element. We take

$$E_h^1 = \{\tilde{\boldsymbol{\tau}}_h \in (L^2(\Omega))_s^4 : \tilde{\boldsymbol{\tau}}_{h|T} \in E_4^1(T) \quad \forall T \in \mathcal{T}_h\} , \quad (11)$$

where $E_4^1(T)$ is the space of tensor-valued functions defined on T , spanned by the following shape functions (cf. (10))

$$\left[\begin{array}{cc} \alpha_1 \bar{x} + \alpha_2 \bar{y} & ; \quad (\alpha_2 - \alpha_4) \bar{x} + (\alpha_3 - \alpha_1) \bar{y} \\ \text{symm.} & ; \quad \alpha_3 \bar{x} + \alpha_4 \bar{y} \end{array} \right] \quad \text{with } \alpha_i \in \mathbb{R} . \quad (12)$$

We remark that the enhanced strain modes described in (12) have already been used in [17].

- $T3E4(II)/T3$ element. We take

$$E_h^2 = \{\tilde{\boldsymbol{\tau}}_h \in (L^2(\Omega))_s^4 : \tilde{\boldsymbol{\tau}}_{h|T} \in E_4^2(T) \quad \forall T \in \mathcal{T}_h\} , \quad (13)$$

where $E_4^2(T)$ is the space of tensor-valued functions defined on T , spanned by the following shape functions (cf. (10))

$$\left[\begin{array}{cc} \alpha_1 \bar{x} & ; \quad \alpha_2 \bar{x} + \alpha_3 \bar{y} \\ \text{symm.} & ; \quad \alpha_4 \bar{y} \end{array} \right] \quad \text{with } \alpha_i \in \mathbb{R} . \quad (14)$$

We remark that this choice is not frame invariant. However, a strategy to make the results at least independent of the user's input data is detailed in [17].

We have the following result, whose proof can be found in [1].

Proposition 3.1 *Under suitable regularity hypotheses (see [1]), for both the $T3E4(I)/T3$ and the $T3E4(II)/T3$ element, we have the error estimate*

$$\|\mathbf{u} - \mathbf{u}_h\|_1 + |p - p_h|_0 \leq Ch \quad , \quad |\mathbf{u} - \mathbf{u}_h|_0 \leq Ch^2 . \quad (15)$$

3.2 Numerical tests

We here investigate the computational performances of the elements introduced above. For comparison purposes, in the sequel we also consider the following method

- $Q4E6/Q4$ – Quadrilateral element with piecewise bilinear and continuous approximation for both the displacements and the pressure, enriched by means of the Enhanced Strains proposed in [15] (see also Section 4.2).

Expressing forces and lengths in KN and m , respectively, we consider a fully constrained square block of incompressible material ($\lambda = +\infty$, $\mu = 40$), which occupies the region $\Omega = (-\pi/2, \pi/2) \times (-\pi/2, \pi/2)$. The test consists in choosing a particular body load \mathbf{b} for which the corresponding analytical solution (\mathbf{u}, p) is available.

Fig. 1 shows the generic adopted mesh for undistorted quadrilaterals, distorted quadrilaterals and triangles, respectively.

In the numerical experiments, we choose the number of subdivisions per direction $n = 8, 16, 32, 64, 128$; we also point out that n behaves as h^{-1} .

Moreover, since the body is fully constrained, the pressure is defined up to a constant, which is fixed in our computations by imposing $\int_{\Omega} p_h = 0$.

Finally, the results obtained using the $Q4E6/Q4$ element with distorted meshes are here below labeled with “ $Q4E6/Q4(\text{dist})$ ”.

Setting

$$\begin{aligned} b_1 &= \mu \cos y \sin y (1 - 4 \cos^2 x) - 2xy \cos(x^2 y) \\ b_2 &= -\mu \cos x \sin x (1 - 4 \cos^2 y) - x^2 \cos(x^2 y) , \end{aligned}$$

the analytical solution is:

$$\begin{aligned} u_1 &= -\frac{\cos^2 x \cos y \sin y}{2} \\ u_2 &= \frac{\cos^2 y \cos x \sin x}{2} \\ p &= \sin(x^2 y) . \end{aligned}$$

For all the considered schemes, Figs. 2–4 report the computed relative errors versus n , in log-log scale.

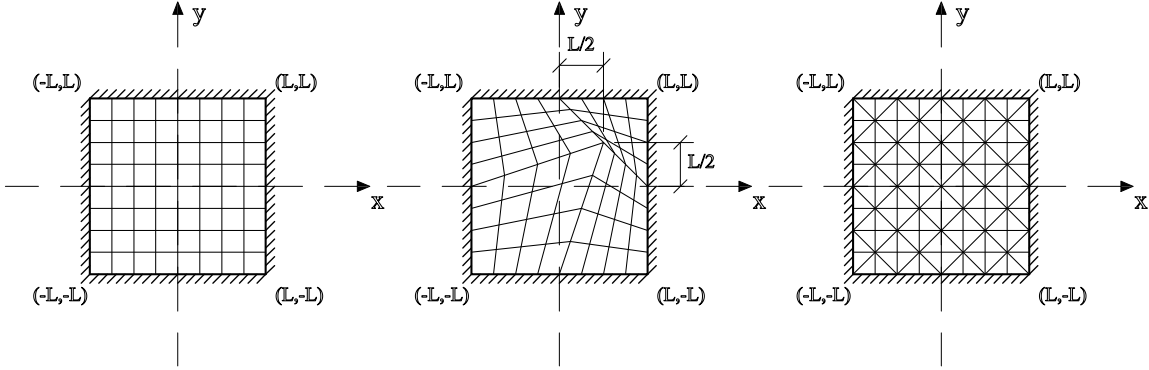


Figure 1: Fully constrained block. Problem geometry and boundary conditions. Undistorted quadrilateral, distorted quadrilateral and triangular meshes.

More precisely, Figs. 2 and 3 show the L^2 -norm convergence rates for \mathbf{u} and p , respectively. Furthermore, Fig. 4 gives the energy-norm convergence rate for \mathbf{u} . The energy-norm is here defined as

$$\|\mathbf{u}\|_{en} := \left(2\mu \int_{\Omega} \boldsymbol{\epsilon}(\mathbf{u}) : \boldsymbol{\epsilon}(\mathbf{u}) \right)^{1/2}, \quad (16)$$

which is clearly equivalent to the H^1 -norm, due to Korn's inequality. For all the elements under investigation, we observe that the numerical results agree with the theoretical predictions. For more numerical tests on the same elements, see [1].

4 A MODEL PROBLEM FOR INCOMPRESSIBLE FINITE DEFORMATION ELASTICITY AND ITS DISCRETIZATION

In this section we analyze a *simple* bidimensional problem which nonetheless shows some of the difficulties arising in general nonlinear elastic problems for incompressible

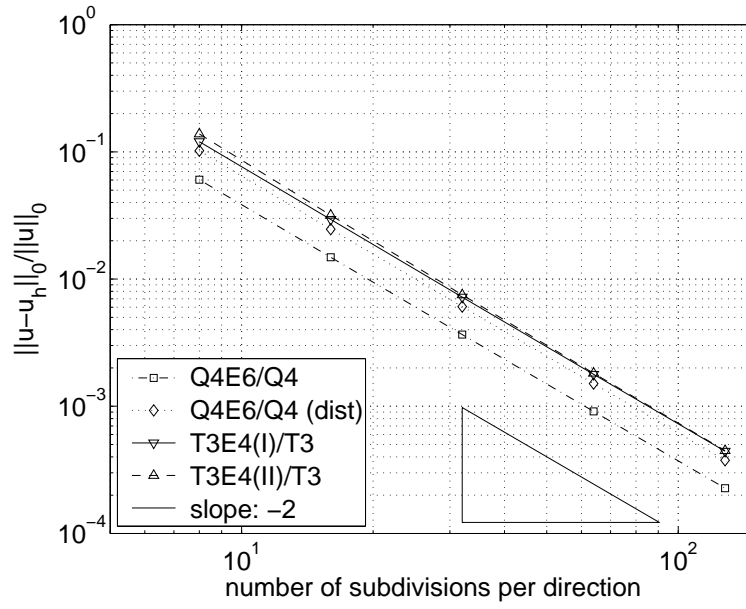


Figure 2: Fully constrained block. L^2 -norm convergence rate for u .

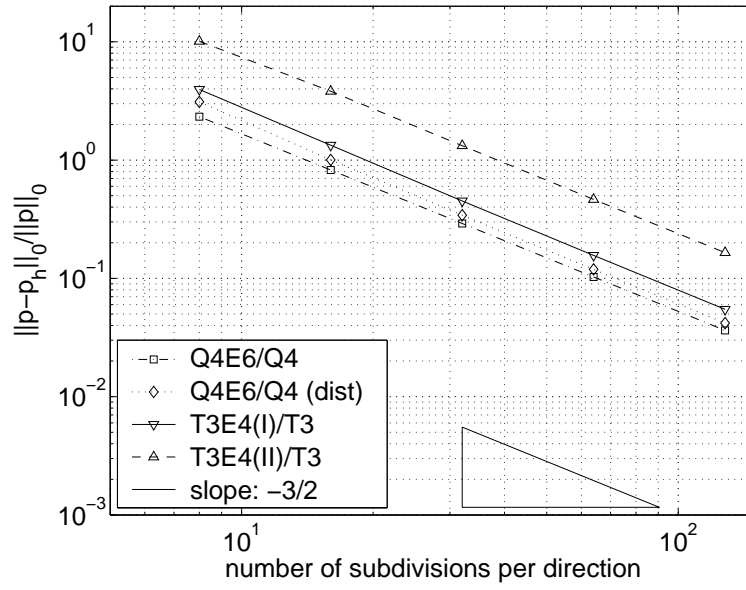
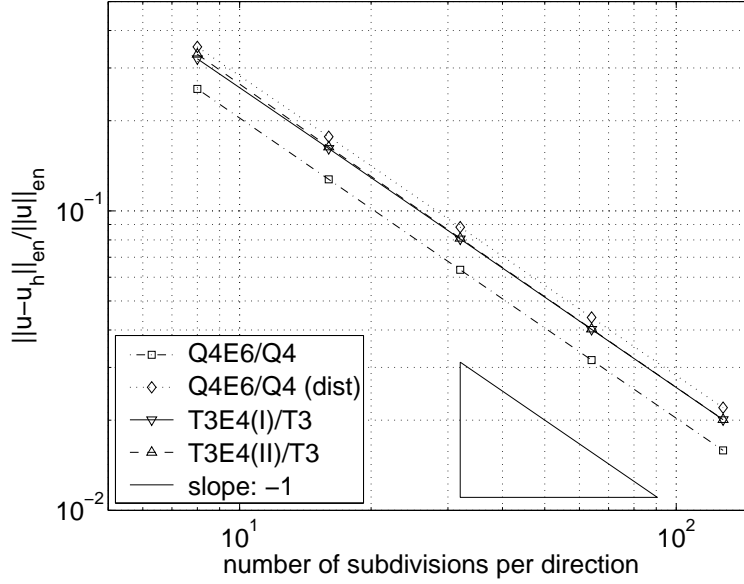


Figure 3: Fully constrained block. L^2 -norm convergence rate for p .


 Figure 4: Fully constrained block. Energy-norm convergence rate for \mathbf{u} .

materials. Using the usual Cartesian coordinates (x, y) , we consider a square material body whose reference configuration is $\Omega = (-1, 1) \times (-1, 1)$; we denote with $\Gamma = [-1, 1] \times \{1\}$ the upper part of its boundary, while the remaining part of $\partial\Omega$ is denoted with Γ_D (cf. Fig. 5). The body Ω is clamped along Γ_D and subjected to the volume force $\mathbf{b} = \gamma \mathbf{f}$, where $\mathbf{f} = (0, 1)^T$ and γ is a real parameter.

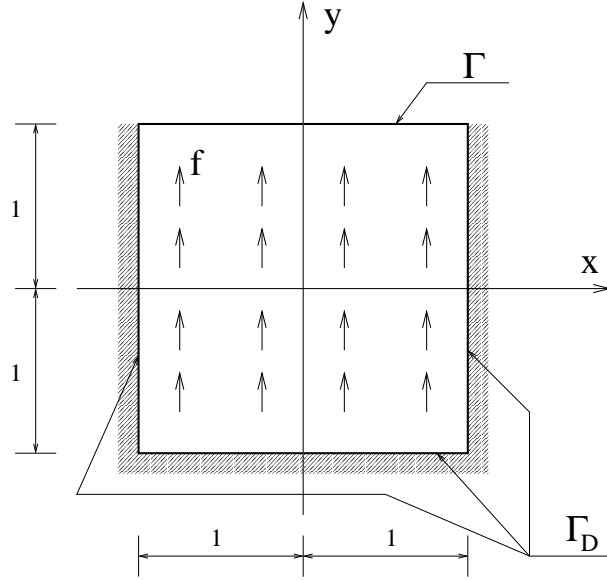
Therefore, the equilibrium problem leads to solve the following variational system (taking the limit for $\lambda \rightarrow +\infty$ in (1))

$$\left\{ \begin{array}{l} \text{Find } (\hat{\mathbf{u}}, \hat{p}) \in \hat{U} \times \hat{P} \text{ such that} \\ \mu \int_{\Omega} \hat{\mathbf{F}} : \nabla \mathbf{v} + \int_{\Omega} (\hat{p} - \mu) \hat{\mathbf{F}}^{-T} : \nabla \mathbf{v} = \gamma \int_{\Omega} \mathbf{f} \cdot \mathbf{v} \quad \forall \mathbf{v} \in U \\ \int_{\Omega} q \ln \hat{J} = 0 \quad \forall q \in P. \end{array} \right. \quad (17)$$

We notice that system (17) constitutes a set of *nonlinear* equations for which a trivial solution can be easily found *for every* $\gamma \in \mathbf{R}$, i.e. $(\hat{\mathbf{u}}, \hat{p}) = (\mathbf{0}, \gamma r)$, where $r = r(x, y) = 1 - y$.

Remark 4.1 *We are not claiming that, for each $\gamma \in \mathbf{R}$, $(\hat{\mathbf{u}}, \hat{p}) = (\mathbf{0}, \gamma r)$ is the only solution of the system.*

Whenever an incremental loading procedure is considered, the passage from γ to $\gamma + \Delta\gamma$ in (17) is typically solved by a Newton's technique. Supposing that at γ convergence has


 Figure 5: Problem domain Ω .

been reached, the first iteration step of Newton's method with initial guess $(\hat{\mathbf{u}}, \hat{p}) = (\mathbf{0}, \gamma r)$ consists (recalling the linearized problem (5) for the case $\lambda = +\infty$) in solving

$$\begin{cases} \text{Find } (\mathbf{u}, p) \in U \times P \text{ such that} \\ 2\mu \int_{\Omega} \boldsymbol{\varepsilon}(\mathbf{u}) : \boldsymbol{\varepsilon}(\mathbf{v}) - \gamma \int_{\Omega} r(\nabla \mathbf{u})^T : \nabla \mathbf{v} + \int_{\Omega} p \operatorname{div} \mathbf{v} = \Delta \gamma \int_{\Omega} \mathbf{f} \cdot \mathbf{v} \\ \int_{\Omega} q \operatorname{div} \mathbf{u} = 0, \end{cases} \quad (18)$$

for every $(\mathbf{v}, q) \in U \times P$. Letting

$$U = \{\mathbf{v} \in H^1(\Omega)^2 : \mathbf{v}|_{\Gamma_D} = 0\} ; \quad P = L^2(\Omega), \quad (19)$$

we consider system (18) as a *model problem* for our subsequent considerations. Denoting with \mathbf{A}^S the symmetric part of a generic second-order tensor \mathbf{A} , introducing the bilinear forms

$$a_{\gamma}(\mathbf{F}, \mathbf{G}) =: 2\mu \int_{\Omega} \mathbf{F}^S : \mathbf{G}^S - \gamma \int_{\Omega} r \mathbf{F}^T : \mathbf{G} \quad , \quad b(\mathbf{v}, q) =: \int_{\Omega} q \operatorname{div} \mathbf{v} , \quad (20)$$

problem (18) can be written in a classical mixed form as

$$\begin{cases} \text{Find } (\mathbf{u}, p) \in U \times P \text{ such that} \\ a_\gamma(\nabla \mathbf{u}, \nabla \mathbf{v}) + b(\mathbf{v}, p) = \Delta \gamma \int_\Omega \mathbf{f} \cdot \mathbf{v} & \forall \mathbf{v} \in U \\ b(\mathbf{u}, q) = 0 & \forall q \in P. \end{cases} \quad (21)$$

4.1 The stability range for the continuous problem

Problem (21) is a typical (parameter-dependent) saddle-point problem. As it is well-established (cf. [7]), the crucial properties for the well-posedness are, together with continuity:

- *the inf-sup condition*, i.e. the existence a positive constant β such that

$$\inf_{q \in P} \sup_{\mathbf{v} \in U} \frac{b(\mathbf{v}, q)}{\|\mathbf{v}\|_U \|q\|_P} \geq \beta ; \quad (22)$$

- *the invertibility on the kernel condition*, i.e. the existence a positive constant $\alpha(\gamma, \mu)$ such that

$$\inf_{\mathbf{v} \in \text{Ker } B} \sup_{\mathbf{u} \in \text{Ker } B} \frac{a_\gamma(\nabla \mathbf{u}, \nabla \mathbf{v})}{\|\mathbf{u}\|_U \|\mathbf{v}\|_U} \geq \alpha(\gamma, \mu) , \quad (23)$$

where

$$\text{Ker } B = \{ \mathbf{v} \in U : b(\mathbf{v}, q) = 0 \quad \forall q \in P \} . \quad (24)$$

As far as the inf-sup condition is concerned, it is a classical result that it holds for the divergence operator. We therefore focus our attention on condition (23), investigating, in particular, the coercivity on $\text{Ker } B$ of $a_\gamma(\cdot, \cdot)$. More precisely, recalling the well-known Korn's inequality, we search for conditions on γ implying the existence of a constant $c(\gamma, \mu) > 0$ such that

$$2\mu \int_\Omega |\boldsymbol{\epsilon}(\mathbf{v})|^2 - \gamma \int_\Omega r (\nabla \mathbf{v})^T : \nabla \mathbf{v} \geq c(\gamma, \mu) \int_\Omega |\boldsymbol{\epsilon}(\mathbf{v})|^2 \quad \forall \mathbf{v} \in \text{Ker } B . \quad (25)$$

We have the following proposition (see [2]).

Proposition 4.2 *Suppose that $\Omega = (-1, 1) \times (-1, 1)$. Then the linearized continuous problem (18) is well-posed and positive-definite on the relevant kernel $\text{Ker } B$ (cf. (25)) if*

$$\gamma \in (-\infty, 3\mu) . \quad (26)$$

Moreover, there exists a $\gamma^* \geq 3\mu$ such that condition (25) fails whenever $\gamma \geq \gamma^*$.

We thus expect that when γ satisfies (26), for the *continuous* problem the trivial solution $(\hat{\mathbf{u}}, \hat{p}) = (\mathbf{0}, \gamma r)$ is unique and stable.

4.2 Discrete stability range for the $Q4E6/Q4$ element

For a finite analysis of problem (17), one should obviously focus on schemes which are reliable at least in the infinitesimal strain regime, otherwise even the first iteration step will fail. This can be accomplished by considering finite element methods satisfying the discrete *inf-sup* condition, as the ones studied in the sequel. Furthermore, since a reliable numerical approximation should be able to correctly reproduce all the stability properties of the continuous problem, it is important to study whether or not a given finite element method satisfies a discrete *coercivity on the kernel* condition, at least for γ in the range shown by (26). With this respect, we consider the enhanced strain $Q4E6/Q4$ element of Pantuso and Bathe (cf. [15]), showing that its stability range is somehow quite different from the continuous problem one. However, we point out that our theoretical analysis is far from being *complete*, although in accordance with the numerical tests presented in Section 4.3. For a comparison with the stability ranges of other well established (and conforming) methods, namely the *MINI* and the $Q2P1$ elements, see [2].

We first recall that the $Q4E6/Q4$ quadrilateral method (which optimally performs in small deformation regimes, as theoretically proved in [11]), is described by the following choice of spaces. For the discretization of the displacement and pressure fields, we take

$$U_h = \{ \mathbf{v}_h \in U : \mathbf{v}_{h|K} \in \mathcal{Q}_1(K)^2 \quad \forall K \in \mathcal{T}_h \} , \quad (27)$$

$$P_h = \{ q_h \in H^1(\Omega) : q_{h|K} \in \mathcal{Q}_1(K) \quad \forall K \in \mathcal{T}_h \} , \quad (28)$$

where $\mathcal{Q}_1(K)$ is the standard space of bilinear functions. Furthermore, the *Enhanced Strain* space is described by

$$E_h = \{ \tilde{\boldsymbol{\tau}}_h \in (L^2(\Omega))^4 : \tilde{\boldsymbol{\tau}}_{h|K} \in E_6(K) \quad \forall K \in \mathcal{T}_h \} . \quad (29)$$

Above, $E_6(K)$ is the space of tensor-valued functions defined on K , spanned by the following shape functions

$$\left[\begin{array}{cc} \alpha_1 \xi + \alpha_2 \xi \eta & ; & \alpha_3 \xi \\ \alpha_4 \eta & ; & \alpha_5 \eta + \alpha_6 \xi \eta \end{array} \right] \quad \text{with } \alpha_i \in \mathbf{R} , \quad (30)$$

where (ξ, η) denotes the standard local coordinates on K .

Therefore, the discretization of problem (18) reads as follows.

Find $(\mathbf{u}_h, \tilde{\boldsymbol{\epsilon}}_h; p_h) \in (U_h \times E_h) \times P_h$ such that:

$$\left\{ \begin{array}{l} 2\mu \int_{\Omega} (\nabla \mathbf{u}_h + \tilde{\boldsymbol{\epsilon}}_h)^S : (\nabla \mathbf{v}_h + \tilde{\boldsymbol{\tau}}_h)^S - \gamma \int_{\Omega} r (\nabla \mathbf{u}_h + \tilde{\boldsymbol{\epsilon}}_h)^T : (\nabla \mathbf{v}_h + \tilde{\boldsymbol{\tau}}_h) \\ + \int_{\Omega} p_h (\operatorname{div} \mathbf{v}_h + \operatorname{tr} \tilde{\boldsymbol{\tau}}_h) = \Delta \gamma \int_{\Omega} \mathbf{f} \cdot \mathbf{v}_h \quad \forall (\mathbf{v}_h, \tilde{\boldsymbol{\tau}}_h) \in U_h \times E_h \\ \int_{\Omega} q_h (\operatorname{div} \mathbf{u}_h + \operatorname{tr} \tilde{\boldsymbol{\epsilon}}_h) = 0 \quad \forall q_h \in P_h . \end{array} \right. \quad (31)$$

Introducing the discrete kernel as

$$K_h = \left\{ (\mathbf{v}_h, \tilde{\boldsymbol{\tau}}_h) \in U_h \times E_h : \int_{\Omega} q_h (\operatorname{div} \mathbf{v}_h + \operatorname{tr} \tilde{\boldsymbol{\tau}}_h) = 0 \quad \forall q_h \in P_h \right\}, \quad (32)$$

we are interested in analyzing for which γ there exists a constant $c_E(\gamma, \mu)$, independent of h , such that (cf. (20))

$$a_{\gamma}(\nabla \mathbf{v}_h + \tilde{\boldsymbol{\tau}}_h, \nabla \mathbf{v}_h + \tilde{\boldsymbol{\tau}}_h) \geq c_E(\gamma, \mu) \int_{\Omega} (|\boldsymbol{\epsilon}(\mathbf{v}_h)|^2 + |\tilde{\boldsymbol{\tau}}_h|^2) \quad (33)$$

for every $(\mathbf{v}_h, \tilde{\boldsymbol{\tau}}_h) \in K_h$.

We have the following result (cf. [2]), which shows that the stability range for the $Q4E6/Q4$ element differs from the continuous problem one (see also Proposition 4.2).

Proposition 4.3 *Consider the case of uniform meshes \mathcal{T}_h formed by equal square elements K with side length h . For the choice (27)–(30), if $\gamma > \mu$ the discrete coercivity on the kernel condition (33) does not hold, provided h is sufficiently small.*

4.3 Numerical tests

We now study the computational performances of the $Q4E6/Q4$ element on the model problem (17). In particular, we wish to numerically detect the stability range and compare such numerical results with the theoretical ones shown in Proposition 4.3 for the *discrete* problem, and in Proposition 4.2 for the *continuous* problem.

The scheme has been implemented in FEAP (see [23]). The model problem is sketched in Fig. 5, and, assuming to express respectively forces and lengths in KN and m , we set $\mu = 40$ and $\mathbf{f} = (0, \gamma)^T$, where γ plays the role of load multiplier. In particular, we find convenient to express the numerical results in terms of the non-dimensional quantity $\tilde{\gamma}$ defined as $\tilde{\gamma} = \gamma L / \mu$ with L some problem characteristic length, in the following set equal to 1 for simplicity and consistent with the model problem. For a given mesh, to detect numerically the element stability range we progressively increase the load multiplier γ , adopting an iterative Newton-Raphson scheme to obtain the solution corresponding to the single load value from the solution corresponding to the previous load value. In particular, we increase the load multiplier until some form of numerical instabilities appears; we indicate the load multiplier corresponding to the appearance of numerical instabilities with γ_{cr} with the corresponding non-dimensional multiplier as $\tilde{\gamma}_{cr}$. To investigate large load multiplier intervals, we adopt different increments $\Delta\gamma$ depending on the load level (Table 1). Clearly, the analyses are performed starting from $\tilde{\gamma} = 0$ for both positive and negative loading conditions, i.e. for $\tilde{\gamma} < 0$ and $\tilde{\gamma} > 0$. Table 2 reports the stability limits and it suggests the following observations.

- The theoretical predictions for the $Q4E6/Q4$ interpolation scheme are that for sufficiently small h the *discrete* problem is unstable for $\tilde{\gamma} > 1$ (cf. Proposition 4.3). The

$\Delta\gamma = 10^{-1}$	$0 \leq \gamma \leq 10^2$
$\Delta\gamma = 1$	$10^2 < \gamma \leq 10^3$
$\Delta\gamma = 10$	$10^3 < \gamma $

Table 1: Load increments $\Delta\gamma$ (depending on the load level γ) for the Newton-Raphson scheme.

mesh	$\tilde{\gamma}_{cr}^-$	$\tilde{\gamma}_{cr}^+$
4×4	-52.8	1.21
8×8	-150	1.07
16×16	-335	0.998
32×32	-723	0.978
64×64	-1480	0.980
128×128	-2980	0.983

Table 2: $Q4E6/Q4$ element: numerical stability limits for the model problem.

results presented in Table 2 seem to indicate that for sufficiently small h the corresponding *numerical* problem is stable for $-\infty < \tilde{\gamma} < 1$ and unstable for $\tilde{\gamma} > 1$. In particular, the stability lower limit is decreasing almost linearly with h , approaching $-\infty$ for $h \rightarrow 0$, while the stability upper limit is about 1 but it does not seem to have a smooth convergence. Accordingly, the numerical results presented in Table 2 confirm the theoretical predictions.

Finally, recalling that the *continuous* problem is stable at least for $-\infty < \tilde{\gamma} < 3$ (see (26)), we may conclude that the $Q4E6/Q4$ interpolation scheme fails in properly detecting the stability range of the continuous problem.

5 CONCLUSIONS

We have reported on some recent results about the numerical approximation of elasticity problems by means on the Enhanced Strain Technique, when applied to the displacement/pressure variational formulation. On one hand, we have proposed two triangular schemes which are stable and optimally convergent in the context of the small deformation regime and for (nearly-)incompressible materials. On the other hand, we have presented a simple model problem which can be useful to investigate the stability of finite element schemes in the finite strain framework. We however notice that the finite element approximation of large deformation problems demand a deeper analysis.

Acknowledgments. This work has been partially supported by the European Project HPRN-CT-2002-00284 “New Materials, Adaptive Systems and their Nonlinearities. Modelling, Control and Numerical Simulation”.

REFERENCES

- [1] F. Auricchio, L. Beirão da Veiga, C. Lovadina and A. Reali. Triangular enhanced strain elements for plane linear elasticity. *Comput. Meth. Appl. Mech. Engrg* (submitted).
- [2] F. Auricchio, L. Beirão da Veiga, C. Lovadina and A. Reali. A stability study of some mixed finite elements for large deformations elasticity problems. *Comput. Meth. Appl. Mech. Engrg* (submitted).
- [3] F. Armero. On the locking and stability of finite elements in finite deformation plane strain problems. *Computers and Structures*, **75**, 261–290, 2000.
- [4] K.J. Bathe. *Finite Element Procedures*. Prentice Hall, Englewood Cliffs, NJ, 1996.
- [5] D. Braess. Enhanced assumed strain elements and locking in membrane problems. *Comput. Meth. Appl. Mech. Engrg.*, **165**, 155–174, 1998.
- [6] J. Bonet and R.D. Wood. *Nonlinear Continuum Mechanics for Finite Element Analysis*. Cambridge University Press, 1997.
- [7] F. Brezzi and M. Fortin. *Mixed and hybrid Finite Element Methods*. Springer-Verlag, New York, 1991.
- [8] P.G. Ciarlet. *Mathematical Elasticity. Volume 1: Three dimensional elasticity*. North-Holland, Amsterdam, 1998.
- [9] T.J.R. Hughes. *The Finite Element Method*. Dover Publications, NY, 2000.
- [10] P. Le Tallec. *Numerical methods for nonlinear three-dimensional elasticity*. In: Handbook of Numerical Analysis, Vol III, 465–622, 1994.
- [11] C. Lovadina. Analysis of strain-pressure finite element methods for the Stokes problem. *Numer. Methods for PDE's*, **13**, 717–730, 1997.
- [12] C. Lovadina, F. Auricchio. On the enhanced strain technique for elasticity problems. *Computers and Structures*, **81**, 777–787, 2003.
- [13] J.E. Marsden and T.J.R. Hughes. *Mathematical Foundations of Elasticity*. Dover Publications, NY, 1993.
- [14] J.C. Nagtegaal and D.D. Fox. Using assumed enhanced strain elements for large compressive deformation. *Int. J. Solids Structures* **33**, 3151–3159, 1996.
- [15] D. Pantuso and K.J. Bathe. A four-node quadrilateral mixed-interpolated element for solids and fluids. *Math. Models Methods Appl. Sci.* **5**, 1113–1128, 1995.

- [16] D. Pantuso and K.J. Bathe. On the stability of mixed finite elements in large strain analysis of incompressible solids. *Finite Elements in Analysis and Design*, **28**, 83–104, 1997.
- [17] R. Piltner and R.L. Taylor. Triangular finite elements with rotational degrees of freedom and enhanced strain modes. *Computers and Structures* **75**, 361–368, 2000.
- [18] B.D. Reddy and J.C. Simo. Stability and convergence of a class of enhanced strain methods. *SIAM J. Numer. Anal.*, **32**, 1705–1728, 1995.
- [19] S. Reese, M. Küssner and B.D. Reddy. A new stabilization technique for finite elements in non-linear elasticity. *Int. J. Numer. Meth. Engng.*, **44**, 1617–1652, 1999.
- [20] S. Reese and P. Wriggers. A stabilization technique to avoid hourglassing in finite elasticity. *Int. J. Numer. Meth. Engng.*, **48**, 79–109, 2000.
- [21] J.C. Simo and F. Armero. Geometrically nonlinear enhanced strain mixed methods and the method of incompatible modes. *Int. J. Numer. Meth. Engng.*, **33**, 1413–1449, 1992.
- [22] J.C. Simo and M.S. Rifai. A class of mixed assumed strain methods and the method of incompatible modes. *Int. J. Numer. Meth. Engng.*, **29**, 1595–1638, 1990.
- [23] R.L. Taylor. FEAP: *A Finite Element Analysis Program, Programmer Manual*. (<http://www.ce.berkeley.edu/~rlt/feap/>).
- [24] P. Wriggers and S. Reese. A note on enhanced strain methods for large deformations. *Comput. Methods Appl. Mech. Engrg.*, **135**, 201–209, 1996.